Glassy relaxation in a de Vries smectic liquid crystal consisting of bent-core molecules

Vishnu Deo Mishra,[1] G. Pratap,[2,*] and Arun Roy[1,†]

[1]*Soft Condensed Matter Group, Raman Research Institute, C. V. Raman Avenue, Sadashivanagar, Bangalore 560080, India*

[2]*Polymer Science and Technology, CSIR-Central Leather Research Institute, Chennai 600020, India*

(Received 28 June 2023; accepted 2 February 2024; published 26 February 2024)

We report experimental investigations of a liquid crystal comprising thiophene-based achiral bent-core banana shaped molecules. The compound exhibits the following phase sequence on cooling: Isotropic (517.4 K), *N* (514.9 K), de Vries SmA (402 K), SmC. Practically no layer contraction was observed across the SmA to SmC transition, confirming the "de Vries" nature of the SmA phase. Interestingly, the crystallization does not occur on cooling the sample, unlike most other liquid crystals. Instead, the SmC phase undergoes a glass transition at 271 K even at a slow cooling rate. The dielectric spectroscopy studies carried out on the sample reveal the presence of a dielectric mode whose relaxation process is of the Cole-Cole type. The relaxation frequency of the mode was found to drop rapidly with decreasing temperature, confirming the glassy behavior. The variation of relaxation frequency with temperature follows the Vogel-Fulcher-Tammann equation, indicating the fragile glassy nature of the sample. This report identifies a bent-core liquid crystal exhibiting a "de Vries" SmA phase and glassy behavior at lower temperatures.

DOI: 10.1103/PhysRevE.109.024703

I. INTRODUCTION

Liquid crystals (LCs) comprise molecules with strong shape anisotropy, and they exhibit long-range orientational order with or without partial translation order. Thus, LCs have the characteristics of crystals while retaining the fluidity of ordinary liquids [1]. The most commonly observed liquid crystalline phases are known as *nematic* and *smectic* phases. The nematic (N) phase has long-range orientational order of the constituent molecules with no translational ordering. The average orientation of the molecular long axes is defined by the unit vector $\hat{n}$ and is known as the director. In the lamellar smectic phases, the anisotropic molecules stack to form layers with translational order along the layer normal $\hat{k}$ but fluid-like order in the layers. The nano-segregation of the electron-rich aromatic core and aliphatic chains of the constituent molecules give rise to such layered structures. In the smectic A (SmA) phase, the director $\hat{n}$ is parallel to the layer normal $\hat{k}$ with the layer spacing d of the order of molecular length l. In the smectic C (SmC) phase, the director $\hat{n}$ tilts away from the layer normal $\hat{k}$ by a tilt angle θ with a layer spacing d less than the molecular length l. The tilt angle $\theta = \cos^{-1}(d/l)$ is generally found to be temperature dependent in the SmC phase. There is usually a significant reduction of the layer spacing across the transition from the SmA to SmC phase, as depicted in Fig. 1. The SmA phase acquires a so-called "bookshelf geometry" when confined between parallel bounding plates treated for homogeneous planar alignment of the molecules. In the bookshelf geometry, the constituent molecules align homogeneously on the bounding plates, giving rise to the layers perpendicular to the plates. Across the SmA-SmC transition, the reduction of layer spacing in bookshelf geometry leads to the buckling of layers, resulting in the so-called chevron structure [2]. The chevron structure originates due to a mismatch between the smectic layer spacing in bulk and at the surface [2,3]. The chevron formation causes various types of defects, such as zig-zag defects, which have been a challenging problem for surface-stabilized ferroelectric LC displays [2,4,5]. This issue can be addressed using materials with no layer contraction across the SmA-SmC transition. Such a SmA phase is known as the "de Vries smectic A" phase. Henceforth, in our discussion, we shall denote the de Vries SmA phase as the "dSmA" phase. De Vries first proposed a model structure for this type of SmA phase where molecules in a layer are tilted with respect to the layer normal but with random azimuthal tilt directions. The random distribution of the tilt direction makes this phase optically uniaxial about the layer normal, which is a characteristic feature of the SmA phase. This model structure is termed a diffuse cone model of the dSmA phase [6,7]. Across the transition from the dSmA to the SmC phase, the already tilted molecules in the layers in the dSmA phase choose a particular azimuthal orientation in the SmC phase with practically no layer contraction, as shown in Fig. 1. A large number of materials consisting of calamatic (rodlike) molecules have been reported to exhibit the dSmA phase [5,8–11]. But only a few bent-core banana shaped molecules are found to exhibit the dSmA phase [12–16].

Bent-core (BC) liquid crystals have attracted significant attention in recent years due to their remarkably distinct optical and electro-optical properties arising from the interplay between polarity and chirality [17–20]. The bent shape enables the molecules to form a lamellar structure with aligned bending directions, giving rise to layer polarization and thus forming ferro- and antiferroelectric phases [17]. Apart from

*Present address: Academy of Scientific and Innovative Research (AcSIR), Ghaziabad 201002, India.

†Corresponding author: aroy@rri.res.in

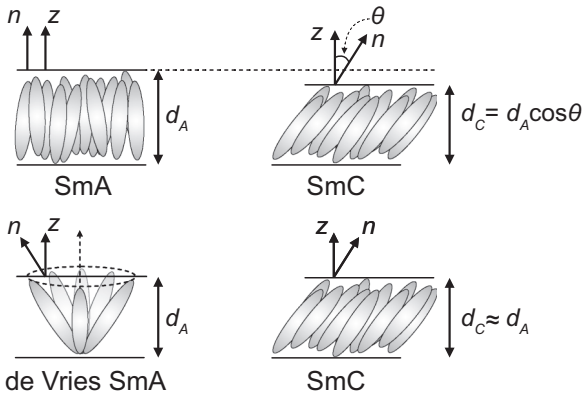

FIG. 1. Schematic representation of the molecular arrangement in conventional SmA, SmC, and de Vries SmA phases comprising calamitic molecules. In the dSmA phase, the molecules are on average tilted away from the layer normal by a significantly large angle with their long axes randomly distributed on a cone according to the diffuse cone model proposed by de Vries [7].

a potential candidate in electro-optic applications due to their fast response time [20], the BC molecules exhibit a rich variety of phases, such as the orthogonal polar smectic SmAP phase [21–23], polarization modulated structures [24–27], nonpolar undulated layer structure [28], dark conglomerate phase [29], and columnar phases [30–32].

A number of studies have been carried out on molecular dynamics and glass formation of calamatic liquid crystals [33–39], but glass-forming bent-core liquid crystals are rarely reported [40]. The formation of a glassy state is often found in various natural phenomena [41–44]. It is also vital for numerous applications, including pharmaceutical [45], food processing [46], polymers [47], and the preservation of insect life under dehydration [48], among others [48–51]. In addition, the glass transition is a long-standing fundamental problem yet to be properly understood [52,53]. The glass formation can take place by many routes [54], a conventional one of which is rapid enough cooling of a liquid phase to avoid the nucleation and growth process of crystals. The liquid appears frozen on the timescale of experimental observation. Although rapid cooling is required for glass formation in many liquids, some organic liquids [55], polymers [54], and liquid crystals [56] can exhibit glass transition at a moderate cooling rate. In the glass-forming liquid crystals, the order can be frozen by preserving the director by external means, such as strong anchoring or applied electric/magnetic field, while cooling the system. This allows the formation of partially ordered glasses retaining all the qualitative features of the liquid crystal phase, which could be exploited in possible applications such as wave plates, holography, and optical storage [35]. Recently it has been pointed out that for some materials, a smectic transition from a high-temperature nematic phase can be frustrated or completely circumvented to produce glasses with tunable liquid crystalline order that can be utilized in organic electronic applications [57,58].

In this paper we investigate the physical properties of liquid crystalline phases of an achiral thiophene-based bent-core liquid crystal using various experimental techniques. The compound exhibits a high-temperature short-range nematic phase followed by two long-range smectic phases. We report two key findings from our experimental studies. First, we find that the higher temperature smectic phase is the dSmA phase, which transits to the SmC phase on decreasing temperature with practically no layer contraction. Unlike the typical BC liquid crystals, both smectic phases are nonpolar with calamatic-type phase behavior. Second, both smectic phases show a dielectric relaxation mode whose relaxation frequency decreases sharply on lowering the temperature, suggesting a glassy behavior. The dielectric relaxation of the mode is of the Cole-Cole type, and the temperature variation of the relaxation frequency follows the empirical Vogel-Fulcher-Tammann (VFT) equation. This suggests the *fragile* nature of the glass for our sample with fragility parameter $D \approx 3$ [54]. The calorimetric studies further confirmed the glass transition at a temperature of about 271 K, which qualitatively agrees with the dielectric studies. We propose a simple model structure for the dSmA phase to account for the experimental observations. To our knowledge, this is the first report of a bent-core liquid crystal exhibiting a dSmA phase and showing glassy behavior.

II. EXPERIMENTAL

Polarized optical microscopy (POM) investigations of the sample were conducted using an Olympus BX 50 microscope equipped with a hot stage (Linkam LTS420E) and a digital camera (Canon EOS 80D). For homeotropic alignment of the molecules, a thin sample was sandwiched between a clean glass slide and a glass cover slip. In addition, commercially available LC cells (INSTEC Inc.) were employed for the planar and homeotropic alignment of the sample. The thickness of these cells was chosen to be 5 μm and 9 μm. The LC cells contain indium tin oxide (ITO)-coated glass plates serving as electrodes for electro-optic and dielectric studies. The sample was introduced into the LC cell by capillary action in its isotropic phase using a hot plate. The electric polarization of the sample in the LC phases was investigated using a triangular wave voltage technique [59] with varying amplitudes and frequencies for planar as well as homeotropically aligned samples. The current response of the sample was measured by monitoring the voltage drop across a 1 kΩ resistor connected in series with the sample cell.

The differential scanning calorimetry (DSC) studies were carried out using Mettler Toledo DSC 3. The sample with a weight of about 2.56 mg was kept in an aluminum crucible, and another empty aluminum crucible was utilized as a reference. The DSC thermogram was recorded at different rates in both the heating and cooling cycles.

To evaluate the effective birefringence of a planar-aligned sample, we measured the variation of average intensity transmitted through the sample as a function of temperature. The planar-aligned sample was kept on the microscope stage at an angle of maximum transmittance between crossed polarizers, and images were taken with varying temperatures by introducing a red filter of wavelength 700 nm in the light path. The average transmitted intensity was computed from the POM images using MATLAB.

The steady-state field-induced electro-optical response of a planar-aligned sample was measured using a He-Ne laser with the application of a triangular ac voltage. The sample was kept between crossed polarizers at an orientation of maximum transmittance, and the transmitted intensity was recorded using a low-noise high-gain photodiode connected to a mixed signal oscilloscope (Agilent Technologies MSO6012A). The intensity was normalized using $I_{\text{nor}} = (I - \bar{I})/\bar{I}$, where I is the measured transmitted intensity through the sample, and $\bar{I}$ is the mean value of the transmitted intensity.

Variable temperature x-ray diffraction (XRD) measurements were conducted using a DY 1042-Empyrean (PANalytical) diffractometer with CuK_α radiation of wavelength 1.54 Å and a PIXcel 3D detector. The samples were filled in Lindemann capillary tubes with an outer diameter of 1 mm. The XRD intensity profiles were measured at different temperatures on cooling the sample from its isotropic phase.

Dielectric measurements were performed on the sample filled in a commercially available LC cell using a high-performance impedance analyzer (Novocontrol Alpha-A) in the frequency range of 1 Hz to 10 MHz. The measurements were limited to 1 Hz due to the dominating charge current contribution at lower frequencies. A sinusoidal ac voltage with an rms amplitude of 0.5 V was used during the dielectric measurement without applying a bias voltage. The temperature of the sample was monitored using a homemade temperature controller with temperature stability of 0.1 K. However, the maximum temperature that can be attained using this setup is 423 K. Therefore, to study the variation of the dielectric constant of the sample in the higher temperature range, a complimentary custom-made dielectric setup with a frequency range of 1 Hz to 100 kHz was employed. The temperature of the sample was monitored by a microscope hot stage and a controller (Instec Inc.). In this setup, a sinusoidal ac voltage of rms amplitude 0.5 V was applied to the sample cell, and a resistance of 1 kΩ connected in series. A lock-in amplifier (Stanford Research SR830) was utilized to measure the amplitude and phase of the voltage drop across the 1 kΩ resistance. The impedance analysis was used to determine the capacitance of the LC cell with and without the sample. The ratio of these measured capacitances gives the effective dielectric constant of the sample.

III. RESULTS AND DISCUSSION

A. Phase sequence

The sample used for our experimental studies is 2,5-bis(4′-(octyloxy)-[1, 1′-biphenyl]-4-yl)thiophene-3-carbonitrile and is denoted as BTCN8. The chemical characterization and preliminary studies of this compound have already been published [60]. The molecule has a bent-core banana shape with a central thiophene ring, as depicted in Fig. 2(a). The opening angle and the molecular length, calculated from the energy minimized molecular structure, are about 143° and 43.5 Å, respectively. A strongly polar carbonitrile group attached to the central thiophene ring enhances the net dipole moment of the molecule at an angle to the long axis [60].

Differential scanning calorimetry (DSC) studies were performed on the sample to detect the various phase transitions

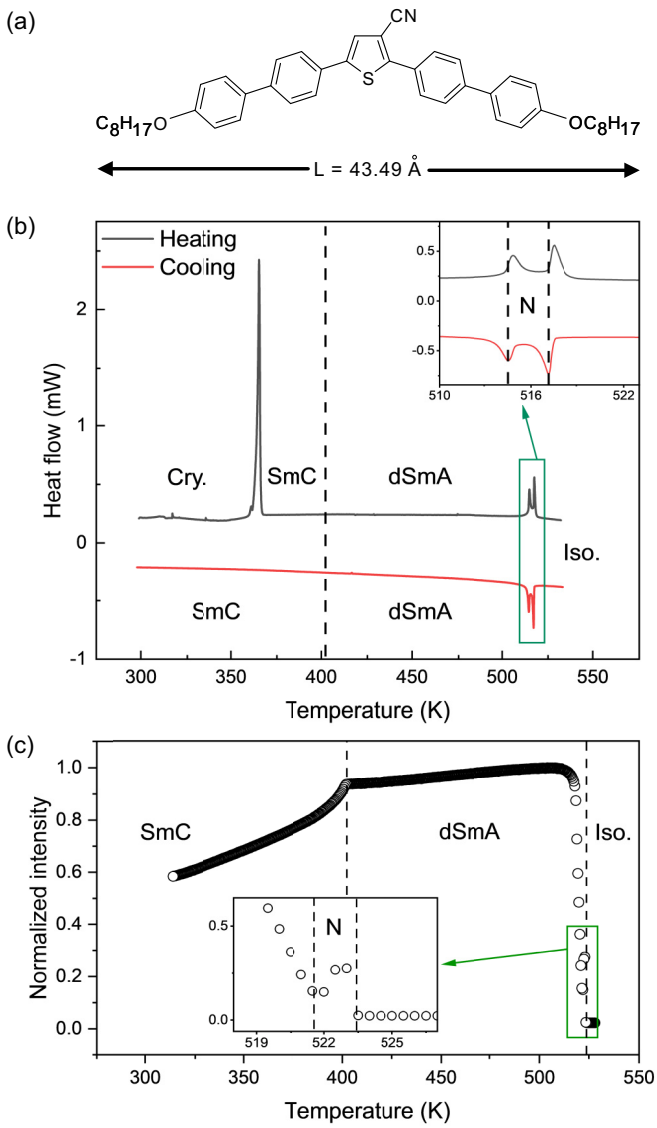

FIG. 2. (a) Molecular structure of the compound BTCN8. (b) DSC thermogram of the compound BTCN8 with heating and cooling rate of 5 K/min. The inset demonstrates the existence of a small-range nematic phase. The sample does not crystallize on cooling to room temperature. The mesomorphic properties of the sample were retained for several weeks, and the melting transition was observed only on the first heating. (c) The temperature variation of the optical transmittance through a planar-aligned sample of thickness 5 μm kept between crossed polarizers while cooling from the isotropic phase. The optical transmittance clearly detects the following phase transition sequence: Isotropic (523.5 K), N (521.5 K), dSmA (402 K), SmC. The inset reveals the existence of a nematic phase with a small range of temperature. All observed phases are enantiotropic.

in heating and cooling cycles at a rate of 5 K/min. The DSC thermogram reveals that the sample melts while heating at 365 K, which, on further heating, shows two transition peaks at 515.9 K and 518.6 K and goes to the isotropic phase. On cooling from the isotropic phase, two transitions were observed at 517.4 K and 514.9 K, and no other transitions were observed on further cooling the sample to room temperature.

The inset in Fig. 2(b) shows the expanded view of the two closely spaced transitions. There is a small hysteretic shift in the transition temperatures between heating and cooling for both isotropic to nematic and nematic to SmA transitions, as expected for the first-order transition. Thus, the DSC thermogram clearly indicates the existence of two mesophases for the compound BTCN8 below its isotropic phase. However, detailed polarizing optical microscopy (POM) studies detect another transition at 402 K while cooling the sample. In POM studies, the optical transmittance through a planar-aligned 5 μm thick sample kept between crossed polarizers was measured while cooling from the isotropic phase. The rubbing direction of the sample cell was kept at an angle of 45° from the polarizer direction for maximum transmittance. Figure 2(c) displays the normalized transmitted intensity as a function of temperature, which clearly detects all the phase transitions. The inset of Fig. 2(c) shows the existence of the short-range nematic phase. The discontinuous change in the slope of the transmitted intensity curve at 402 K corresponds to an additional phase transition. Based on the experimental studies, we identify the following phase sequence for the compound BTCN8 on cooling to room temperature:

$$\text{Isotropic} \xrightarrow{517.4\,\text{K}} \text{N} \xrightarrow{514.9\,\text{K}} \text{de Vries SmA} \xrightarrow{402\,\text{K}} \text{SmC}.$$

All the observed mesophases are found to be enantiotropic. The absence of a DSC peak across the dSmA to SmC phase transition indicates the second-order nature of this transition. The SmC phase became increasingly viscous on lowering the temperature while retaining the fluidity to room temperature. The sample did not crystallize on cooling. Instead, a glass transition was observed at 271 K, which will be discussed later.

B. X-ray diffraction studies

The variable temperature x-ray diffraction (XRD) studies were carried out at various temperatures to investigate the molecular organization in the observed liquid crystalline phases. In the highest temperature short-range nematic phase, a single diffuse peak was observed in the wide-angle region with no sharp peak at the small-angle region, which is characteristic of the Nematic phase. In the dSmA and SmC phases, the XRD intensity profiles as a function of the scattering vector q are shown in Fig. 3(a). In both of these phases, two sharp peaks were observed in the small-angle region at q values in the ratio of 1:2. In addition, a diffused broad peak was observed in the wide-angle region centered about $q = 1.36$ Å^{-1} and $q = 1.43$ Å^{-1} in the dSmA and SmC phases, respectively. The shifting of the maximum of the wide-angle diffuse peak towards a higher value of q on cooling is due to increased molecular packing density. The XRD results indicate a lamellar molecular organization with liquid-like order within the layers. The layer spacings calculated from the XRD data in the dSmA and SmC phases are 38.39 Å and 38.29 Å, respectively, which do not vary appreciably with temperature. The molecular length l of the compound BTCN8 is 43.5 Å, which is significantly larger than the observed layer spacing d in both smectic phases. This indicates that the molecules are tilted within the layers. The tilt angle with respect to the layer normal can be estimated using $\theta = \cos^{-1}(d/l)$. The temperature variation of the tilt angle θ is shown in Fig. 3(b). The tilt angle θ varies slightly across the whole temperature range and attains a shallow minimum value of about 28° near the dSmA to SmC transition. Figure 3(b) also shows the temperature variation of the normalized layer spacing d/d_{ac}, where d_{ac} is the maximum value of layer spacing in the dSmA phase close to the transition. It is clear from Fig. 3(b) that the layer spacing does not change appreciably across the transition from the dSmA to the SmC phase. The layer contraction in the SmC phase at 10 K below the dSmA-SmC transition temperature is only about 0.17%. These observations confirm that the higher temperature smectic phase is a de Vries-type SmA phase. In the dSmA phase, the molecules are tilted within the layers, having a uniform azimuthal distribution of their tilt directions, giving rise to an optically uniaxial texture about the layer normal. In contrast to the conventional SmA phase, the layer spacing in the dSmA phase is significantly less than the molecular length. The large opening angle of the bent structure of the BTCN8 molecules and a strong dipole moment due to the polar cyano group projecting in the lateral direction perhaps favor the tilted nonpolar molecular organization in the layers [61].

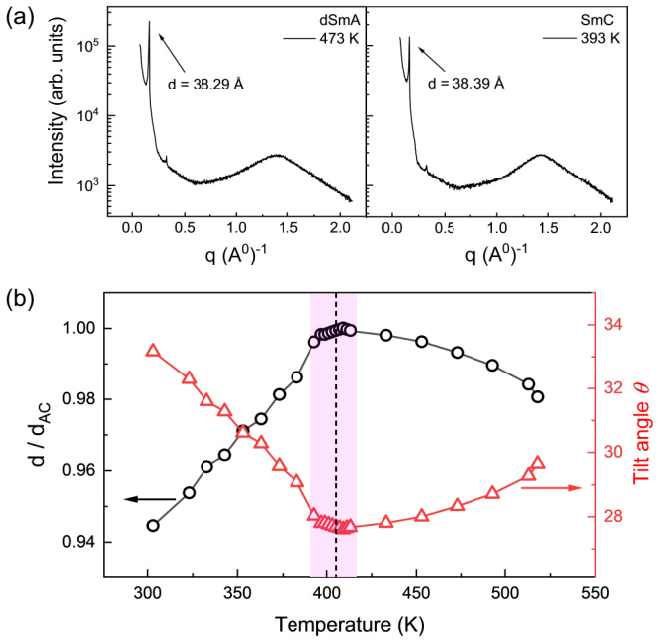

FIG. 3. (a) XRD intensity profile for the compound BTCN8 in dSmA and SmC phases at temperatures 473 K and 393 K, respectively. (b) The temperature variation of the ratio d/d_{ac} and tilt angle θ were obtained from the XRD data and estimated molecular length. The layer thickness remains almost unchanged across the dSmA-SmC transition, showing the de Vries nature of the SmA phase. The vertical dotted line indicates the dSmA to the SmC transition temperature. Across the transition depicted by the pink shaded region, the layer contraction is only about 0.17%. The error bars are smaller than the size of the symbols.

Across the transition from the dSmA to the SmC phase, the random directions of the already tilted molecules get correlated, giving rise to a uniformly tilted configuration with no considerable change in the layer thickness. It can be seen from Fig. 3(b) that the layer spacing is maximum near the

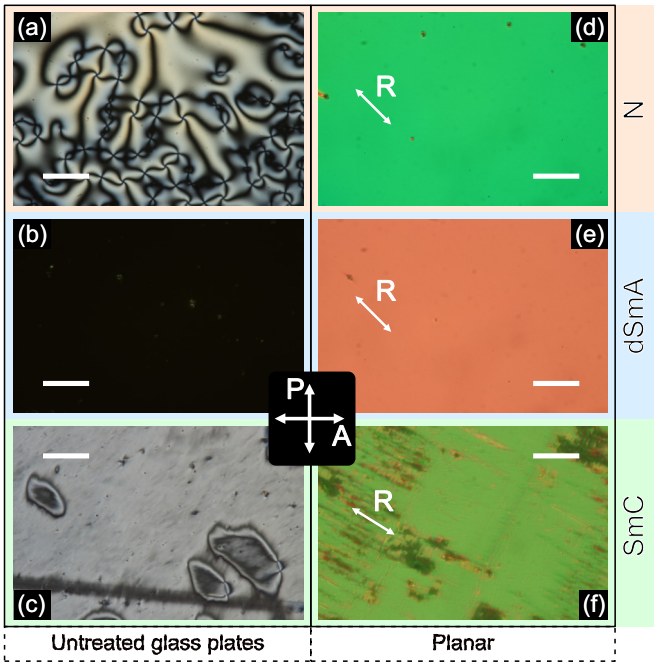

FIG. 4. POM texture of homeotropically aligned thin sample kept between a clean glass plate and a cover slip at (a) 522 K, (b) 518 K, and (c) 388 K and that of the planar-aligned sample of thickness 5 μm at (d) 522 K, (e) 508 K, and (f) 333 K. The POM textures were taken under crossed polarizers conditions while cooling the samples from their isotropic phase. ***R*** indicates the rubbing direction, and the crossed arrows denote the positions of the polarizers. The scale bar represents a length of 50 μm.

dSmA-SmC transition and decreases slightly from this value in the dSmA phase at higher temperatures and in the SmC phase at lower temperatures. The increase in the layer thickness in the dSmA phase with decreasing temperature can be attributed to the stretching of the alkyl chain with increasing packing density. This trend of negative thermal expansion of the layer spacing in the dSmA phase has also been observed in other materials exhibiting de Vries-type SmA phases [9,11]. In our sample, a slight decrease in layer spacing was observed in the SmC phase at lower temperatures. However, the observed layer contraction in the whole temperature range of about 225 K in the dSmA and the SmC phases is only about 5%. The POM studies discussed in the following section further confirmed the de Vries nature of the SmA phase.

C. POM and electro-optic measurements

The POM observations were carried out on different samples to further characterize the different phases. The POM textures were observed between crossed polarizers while cooling the sample from the isotropic phase. For our compound, the sample sandwiched between a clean glass plate and a cover slip tends to align homeotropically. In this preparation, the sample thickness was not controlled. The nematic phase below the isotropic phase exhibits a characteristic schlieren texture as shown in Fig. 4(a). The quasiplanar alignment of the molecules in the nematic phase gives rise to the schlieren texture. Upon cooling to the dSmA phase, the molecules align homeotropically, and the texture appears completely dark, as shown in Fig. 4(b). The dark texture remains invariant on rotating the sample on the microscope stage, confirming the uniaxial nature of the dSmA phase. In the dSmA phase, the layers prefer to orient parallel to the substrate, giving rise to the homeotropic alignment of the molecules. This observation and the intralayer molecular tilt observed in the XRD studies discussed earlier confirm the de Vries nature of the SmA phase. On further cooling, a birefringent schlieren texture was observed in the lower temperature SmC phase as shown in Fig. 4(c). The birefringent schlieren texture in this homeotropic geometry and the layer spacing less than the molecular length observed in XRD studies suggest the tilted smectic order. Only unit strength defects were observed in the schlieren texture of this SmC phase, indicating the synclinic organization of the molecules in the layers.

In a planar-aligned LC cell, the sample aligns homogeneously along the rubbing direction in the nematic and dSmA phases. The textures in the nematic and the dSmA phases are brightest when the rubbing direction is kept at 45° with respect to the polarizer, as shown in Figs. 4(d) and 4(e), respectively. In the dSmA phase, the layers are perpendicular to the glass plates, adopting a so-called bookshelf geometry with an optic axis along the layer normal. The smooth texture of the dSmA phase breaks down into two types of domains as shown in Fig. 4(f) in the lower temperature SmC phase. The degeneracy in the azimuthal tilt orientations of the molecules in the dSmA phase is lifted during the transition to the SmC phase. It leads to the formation of two surface stabilized regions with symmetrically opposite optical tilt, as shown in Fig. S1 of the Supplemental Material [62].

Though the layer thickness and, hence, the molecular tilt do not change appreciably across the dSmA to SmC transition, the increasing correlation of the molecular tilt direction in the SmC phase gives rise to an optic axis away from the layer normal. The angle between the optic axis and the layer normal is defined as the optical tilt angle θ_{opt}. The θ_{opt} of a given domain of a 5 μm thick planar-aligned sample in the SmC phase was measured using POM as a function of temperature. Figure 5(a) shows the variation of θ_{opt} as a function of $(T_{ac} - T)$, where T_{ac} is the dSmA to SmC transition temperature and T is the measured temperature. The inset of Fig. 5(a) depicts the POM texture of two opposite tilted domains under crossed polarizers at 287 K. The rotation angle between dark states in domains of opposite tilt orientations is $2\theta_{\text{opt}}$. As can be seen from the Fig. 5(a), the value of θ_{opt} increases continuously from zero and tends to saturate at lower temperatures. This increase in the θ_{opt} at (T_{ac}) is suggestive of a second-order transition from the dSmA to the SmC phase. This can be verified by fitting the temperature variation of the θ_{opt} to the power law

$$\theta_{\text{opt}}(T) = \theta_0(T_{ac} - T)^{\beta}, \tag{1}$$

where β is an exponent, which can be related to the nature of the phase transition. The generalized Landau theory predicts $\beta = 0.5$ for second-order transition, whereas $\beta = 0.25$ for a tricritical point corresponding to crossover from second- to first-order transition. The solid line in Fig. 5(a) shows the fit to the experimental data using Eq. (1) with exponent $\beta = 0.255 \pm 0.009$ for our sample. The obtained β value suggests

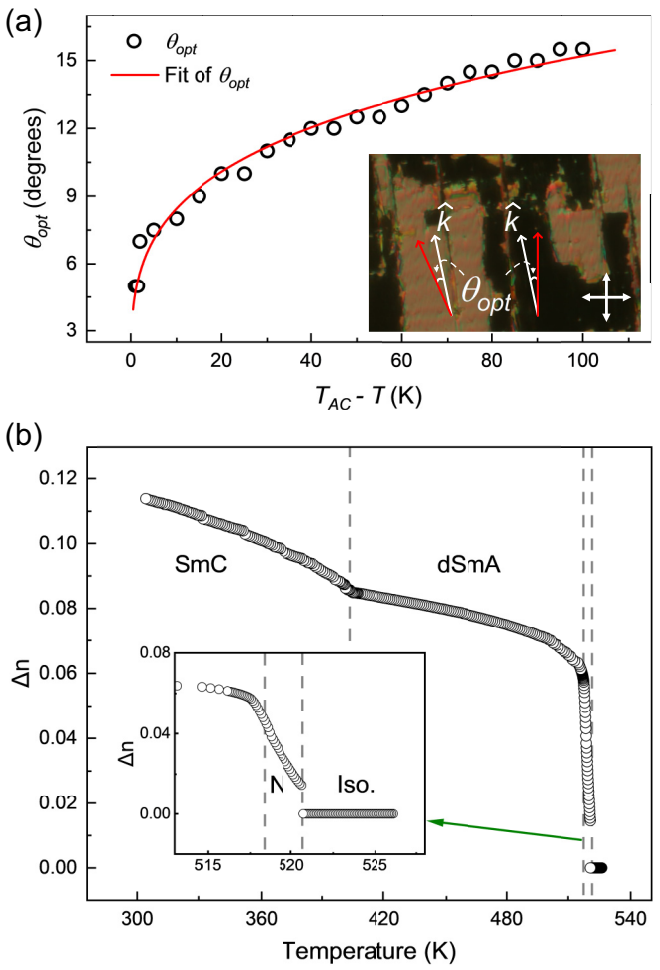

FIG. 5. (a) Variation of optical tilt angle θ_{opt} as a function of $(T_{ac} - T)$ in the SmC phase. The solid line shows the fit to the experimental data using Eq. (1). The inset of (a) shows the oppositely tilted domains in the SmC phase with the layer normal denoted by unit vector $\hat{k}$. In both domains, $\hat{k}$ are parallel, but the optic axes are tilted on the opposite side of $\hat{k}$, giving rise to the optical contrast between crossed polarizers. The white and red arrows represent the direction of the layer normal $\hat{k}$ and the optic axis, respectively, in the two domains. (b) Temperature variation of the effective birefringence (Δn) of a planar-aligned sample while cooling from the isotropic phase. The inset of (b) shows the magnified view of the data in the short temperature range of the nematic phase.

that the dSmA to SmC transition in our sample is close to the tricritical point. The absence of a DSC peak associated with this transition in our sample also suggests that the transition is of second order in nature. Similar values of the exponent β have also been reported for other materials exhibiting dSmA to SmC phase transition [63,64].

We also measured the effective birefringence of a planar-aligned sample of thickness 5 μm as a function of temperature in the liquid crystalline phases. The birefringence was measured by monitoring the transmitted intensity through the sample between crossed polarizers using POM. The transmitted intensity through the sample can be written as

$$I = \frac{I_0}{2}\sin^2(2\Psi)(1 - \cos\Delta\Phi), \tag{2}$$

where I_0 is the intensity of the incident light, Ψ is the angle between the local optic axis and the polarizer, and $\Delta\Phi = (2\pi\,\Delta n d)/\lambda$ is the phase difference introduced by the sample between the ordinary and extraordinary rays. Here d is the sample thickness, λ is the wavelength of the incident light, and Δn is the effective birefringence of the sample. In our experiments, the angle Ψ was set to 45° for maximum transmittance. The details of the experimental method to measure the transmitted intensity are described in Sec. II, and the effective birefringence Δn was calculated using Eq. (2). The variation of Δn as a function of temperature is shown in Fig. 5(b). While cooling from the isotropic phase, a discontinuous jump in the Δn was observed at the isotropic-N transition temperature. The value of Δn continued to increase in the N phase, and a slope change at the N-dSmA transition temperature was observed. The Δn value increases slightly with decreasing temperature and tends to saturate at lower temperatures in the dSmA phase. The Δn again started to increase with decreasing temperature from the dSmA to SmC transition temperature. The low value of the birefringence in the dSmA phase ($\Delta n \approx 0.08$) compared to that of the SmC phase supports the de Vries nature of the SmA phase [5].

Though the transition from the dSmA to the SmC phase is not detected in the DSC measurements, a clear textural change was observed in the homeotropic as well as planar-aligned LC cells at about 402 K. In addition, the temperature variation of the optical tilt angle and the birefringence of the sample also show a clear phase transition at 402 K. These observations confirm the existence of phase transition at 402 K and cannot be explained by other effects, such as surface-induced changes. The second-order nature of this transition accounts for the absence of DSC peak.

The spontaneous electric polarization of the sample in the dSmA and SmC phase was investigated using a triangular wave voltage technique [59]. A voltage of amplitude 50 V was applied across the planar-aligned sample of thickness 5 μm. The current responses of the sample are shown in Fig. S2 [62]. No current peak associated with polarization reversal was observed, indicating that the layers in both smectic phases do not possess spontaneous polarization.

Despite the absence of polarization, a clear reversible field-induced change in the texture was observed in the SmC phase for a planar-aligned sample (see Fig. S3 [62]). The electro-optical response of the planar-aligned sample kept between crossed polarizers was measured in the SmC phase under the application of a triangular wave voltage. The observed optical response was found to be at twice the frequency of applied voltage (see Fig. S4 [62]). This observation also suggests the absence of polarization in the layers. The observed electro-optical response arises due to the quadratic coupling between the applied electric field and the dielectric anisotropy of the sample. No such optical response was found in the dSmA phase with an applied field as high as 20 V/μm.

D. Dielectric studies

The dielectric properties of the samples were investigated using the LC cells for planar alignment. The methods used for the dielectric measurements are described in Sec. II. The effective dielectric constant (ϵ_{eff}) was measured by applying

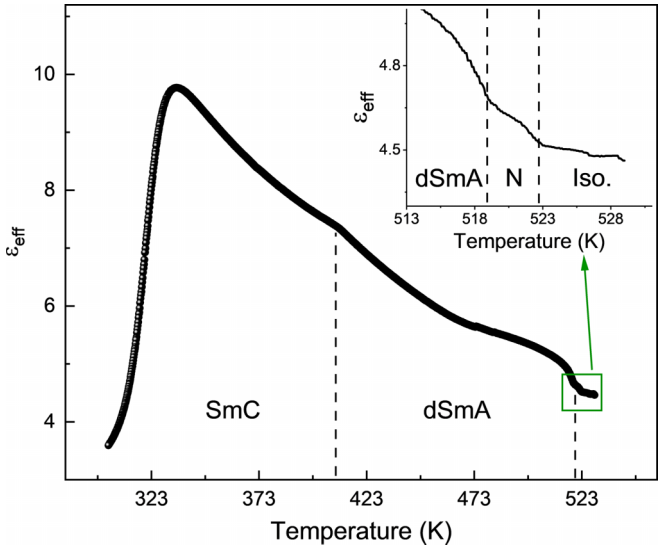

FIG. 6. Variation of the effective dielectric constant (ϵ_{eff}) of the compound BTCN8 in a planar-aligned LC cell of sample thickness 5 μm as a function of temperature. The data clearly detect the various phase transitions and are in agreement with the DSC and POM observations. The dielectric constant's low value indicates the absence of spontaneous polarization in the sample. The inset shows the magnified view of the marked region.

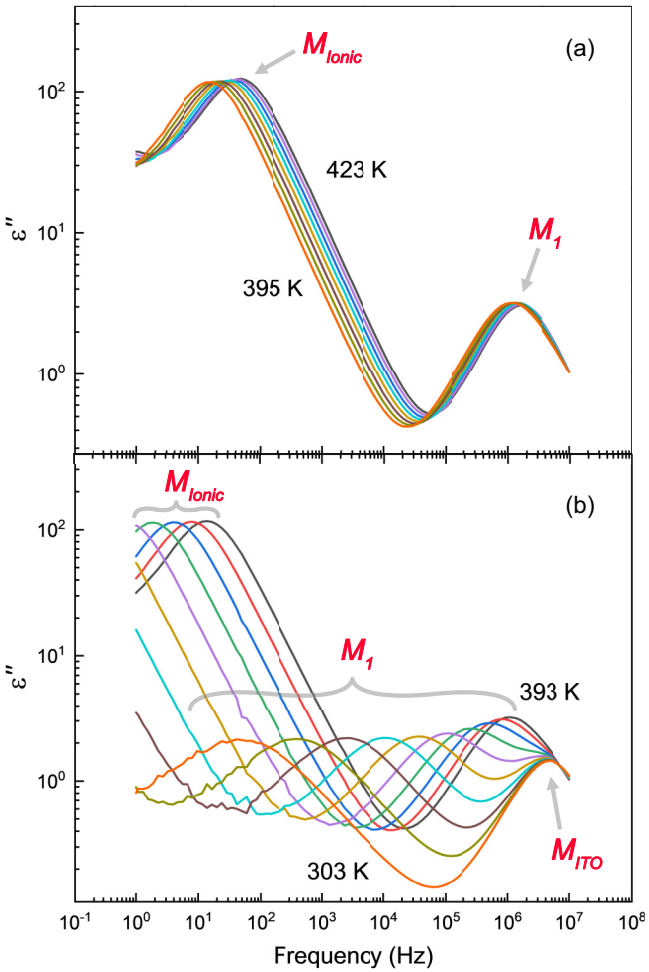

FIG. 7. Variation of the imaginary part of the dielectric constant (ϵ'') as a function of frequency at different temperatures. (a) In the high-temperature range from 423 K to 395 K with a temperature step of 4 K. (b) In the low-temperature range from 393 K to 303 K with a temperature step of 10 K. The peaks in the data represent various dielectric relaxation processes.

a sinusoidal ac voltage of rms amplitude 0.5 V and frequency 5641 Hz while cooling the sample from its isotropic phase. Figure 6 shows the temperature variation of ϵ_{eff} of the sample, which clearly detects the transitions between the observed phases. The transition temperatures agree with the DSC and POM measurements. The increase of ϵ_{eff} in the planar-aligned nematic phase while cooling from the isotropic phase suggests negative dielectric anisotropy of the sample. The ϵ_{eff} continued to increase on further decreasing the temperature to 333 K and sharply decreased below it. This sharp decrease does not correspond to a phase transition. Rather, it occurs due to dielectric relaxation, as discussed later.

To study the dielectric relaxation behavior of the samples, the dielectric permittivity was measured as a function of frequency in the range of 1 Hz to 10 MHz at different temperatures for planar-aligned samples. The frequency dependent complex dielectric permittivity of the sample can be written as

$$\epsilon^*(f) = \epsilon'(f) + i\epsilon''(f), \tag{3}$$

where ϵ' and ϵ'' are real and imaginary parts of the complex dielectric permittivity, respectively, and f being the frequency of the applied field.

The frequency dependence of $\epsilon''(f)$ at different temperatures in the dSmA and SmC phases are shown in Fig. 7. The observed peaks in $\epsilon''(f)$ curve correspond to the relaxation frequency of different dielectric modes of the sample. Figure 7(a) illustrates the frequency dependence of $\epsilon''(f)$ in the high-temperature range from 423 K to 393 K with a temperature step of 4 K. The sample is in the dSmA phase at 423 K, and the transition to the SmC phase occurs at about 403 K. The relaxation peaks in the small frequency range below 100 Hz with relatively high dielectric strength are arising due to the ionic conductivity of the sample and will be ignored in further discussions. Another mode with the relaxation frequency in the MHz range was found in this temperature range, which is denoted as M_1 in 7(a). The intensity of these relaxation peaks remained almost constant, and the peak frequency gradually decreased upon lowering the temperature. The M_1 mode was found to exist in both dSmA and SmC phases and does not vary appreciably across the transition, as can be seen from Fig. 7(a). The frequency dependence of $\epsilon''(f)$ in the lower temperature range from 393 K to 303 K with a temperature step of 10 K is shown in Fig. 7(b). At lower temperatures, the relaxation frequency of mode M_1 started to decrease rapidly with decreasing temperature and attained a value of about 50 Hz at ambient temperature. In this lower temperature range, another weak relaxation peak at about 5 MHz was clearly visible, which did not vary with temperature as shown in Fig. 7(b). This peak, denoted as M_{ITO}, arises due to the finite sheet resistance of the ITO coating used in the LC cell and is masked by the M_1 mode in the higher temperature range.

Similar experiments were carried out on a homeotropically aligned sample, and one relaxation mode was found to exist in the same temperature range as in the planar-aligned sample. The temperature variation of ϵ' for the homeotropic and the planar-aligned sample is shown in Fig. S5 [62]. In the homeotropic LC cell, the molecules acquired a quasihomeotropic alignment with a nonuniform dark texture between crossed polarizers, as shown in Fig. S6 [62]. This nonuniform alignment is probably due to the incompatibility of the strong homeotropic anchoring and the diffuse cone structure of the dSmA phase. The quasihomeotropic alignment of the molecules in the homeotropic cell can be attributed to the presence of mode M_1. Thus, the sample exhibits one dielectric relaxation mode M_1 present in both alignments. The dielectric strength in the homeotropic aligned sample is significantly lower compared to that in the planar cells, indicating that the mesophases possess negative dielectric anisotropy.

In order to analyze the measured dielectric relaxation processes, the dielectric spectra were fitted using the Havriliak-Negami (HN) equation [65,66]. This empirical equation expresses the frequency-dependent complex permittivity ϵ^* in terms of the various relaxation processes given by

$$\epsilon^*(f) - \epsilon_\infty = -\frac{i\sigma_0}{\epsilon_0 \omega^s} + \sum_{j=1}^{n} \frac{\Delta\epsilon_j}{[1 + (i\omega\tau_j)^{\alpha_j}]^{\beta_j}}. \quad (4)$$

In this equation, $\Delta\epsilon_j$ represents the dielectric strength of the jth relaxation process, τ_j represents the corresponding relaxation time, ϵ_∞ represents the high-frequency limit of permittivity, and α_j, β_j are shape parameters. These parameters describe the broadness and asymmetry of the dielectric loss spectra, respectively, and satisfy the conditions $0 < \alpha_j < 1$ and $0 < \alpha_j\beta_j < 1$. The term $i\sigma_0/\epsilon_0\omega^s$ is related to the conductivity, where σ_0 is the direct current (dc) conductivity, ϵ_0 is the permittivity of free space, and s is a fitting parameter that determines the slope of the conductivity. In the case of pure Ohmic conductivity, $s = 1$, while $s < 1$ could be observed in the case of additional influence due to electrode polarization [52]. The HN response reduces to the Cole-Davidson response [67] when $\alpha = 1$, and to the Cole-Cole response [68] when $\beta = 1$. The process under discussion is termed Debye relaxation for both α and β equal to unity.

The dielectric spectra for our sample could be fitted well using Eq. (4). Figure 8(a) shows the variation of $\epsilon''(f)$ as a function of frequency at 333 K along with the fitted curve. The fitting parameters obtained for some temperatures are listed in Table I. The asymmetry parameter $\beta = 1$ for our sample remains almost constant at varying temperatures. This implies that the shape of the dielectric loss peak is symmetric, and the relaxation process is of the Cole-Cole type. The Cole-Cole parameter α was found to be close to 0.68 at lower temperatures and tends to decrease slightly with increasing temperature. This indicates that the width of the dielectric loss spectrum tends to increase with decreasing temperature, as can also be seen from Fig. 7(b). The deviation of experimental data from the fitted curve at higher frequencies in Fig. 8(a) is due to the overlap of the relaxation peak with the additional peak at about 5 MHz arising from the ITO coating of the LC cell. We have also carried out the dielectric measurements on a 9 μm

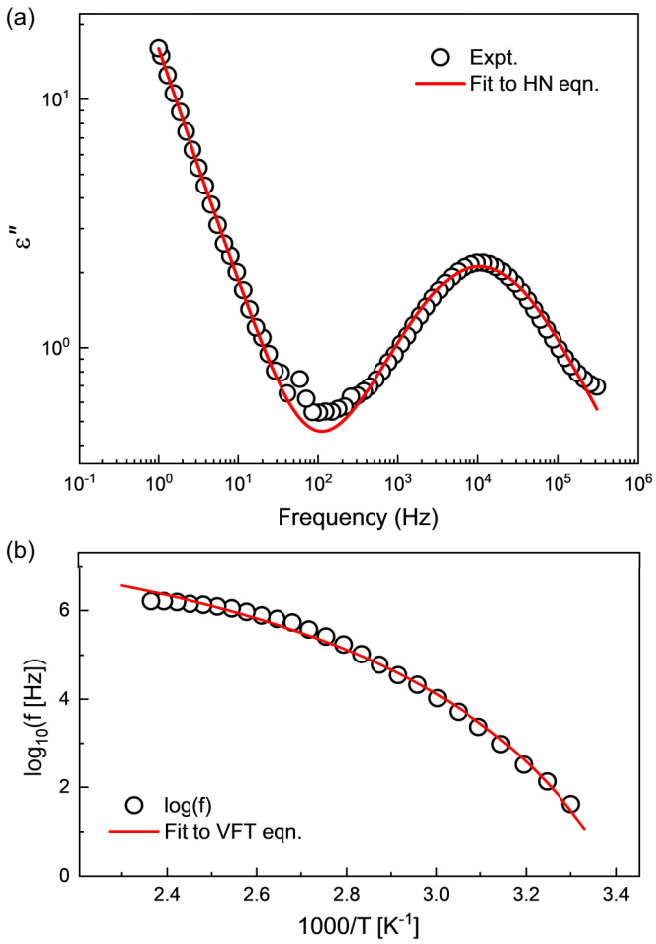

FIG. 8. (a) Frequency variation of ϵ'' at 333 K along with fitted curve (solid line) using Eq. (4). The deviation of the fitted curve in the higher frequency region is due to the overlap of the relaxation peak in the MHz range associated with ITO coating. (b) Relaxation frequency of mode M_1 as a function of inverse temperature. The solid curve represents the fit to the experimental data using VFT Eq. (5), indicating the non-Arrhenius behavior of the liquid.

LC cell. The relaxation frequency of the observed mode M_1 was found to be independent of the sample thickness.

The temperature dependence of relaxation frequency provides a useful classification of glassformers along a "strong" to "fragile" scale [51,54]. The former shows an Arrhenius

TABLE I. The shape parameters α and β, and dielectric strength $\Delta\epsilon$ value obtained from fitting the experimental data with Eq. (4) at different temperatures.

T [K]	α	β	$\Delta\epsilon$
303	0.65 ± 0.02	1 ± 0.08	6.69 ± 0.17
308	0.68 ± 0.01	1 ± 0.06	6.50 ± 0.16
313	0.74 ± 0.02	0.95 ± 0.03	6.44 ± 0.21
318	0.67 ± 0.01	0.99 ± 0.06	7.33 ± 0.07
323	0.68 ± 0.01	1 ± 0.06	7.23 ± 0.06
328	0.67 ± 0.02	1 ± 0.08	7.23 ± 0.07
333	0.68 ± 0.02	1 ± 0.09	7.12 ± 0.08
338	0.69 ± 0.02	1 ± 0.12	7.06 ± 0.11

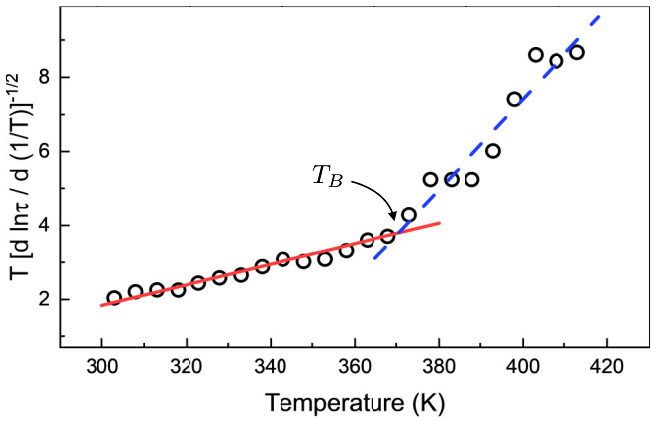

FIG. 9. Linear variation of '$T\ [d(\ln\tau)/d(1/T)]^{-1/2}$' as a function of temperature showing two dynamical regimes separated by the crossover temperature $T_B = 370\,K$. The slope and ordinate of the linear fit in the lower (higher) temperature region are 0.028 and −6.51 (0.123 and −41.65), respectively.

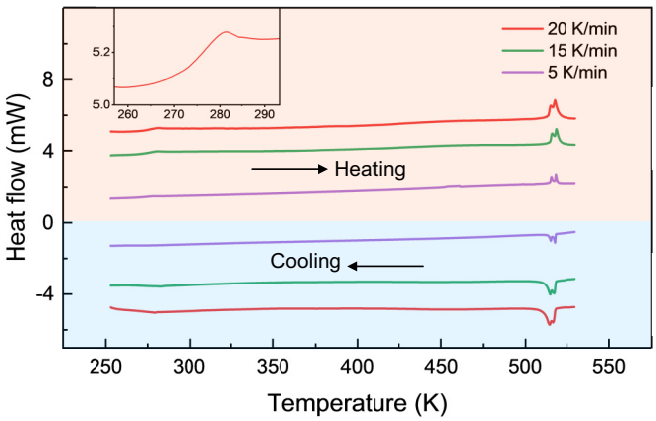

FIG. 10. DSC thermogram of the compound BTCN8 at different rates while cooling from the isotropic phase and subsequent heating. A step change in the curve at a temperature of 271 K is indicative of glass transition. The sample does not crystallize over a few weeks.

dependence, whereas the latter deviates from the Arrhenius behavior. The glass transition is associated with several previtreous phenomena occurring well above the glass transition temperature [69,70]. To describe the previtreous behavior, numerous model relations have been developed [52,53]. The empirical Vogel-Fulcher-Tammann (VFT) equation remains the most popular one among them and is nowadays used in the following form [52]:

$$f = f_\infty \exp\left(-\frac{D\,T_0}{T - T_0}\right), \tag{5}$$

where f_∞ is the preexponential constant, extrapolated Vogel temperature T_0 is usually located below the glass transition temperature T_g, and D is a constant denoting the fragility of the system and describes the degree of deviation away from the basic Arrhenius behavior. The measured relaxation frequency as a function of temperature along with its fit to Eq. (5) is shown in Fig. 8(b). The fitting parameters are $T_0 = 253.15 \pm 0.004$ K, $\log_{10} f_\infty = 8.49 \pm 0.19$, and $D = 3.19 \pm 0.39$. Such a large D value indicates the highly fragile glassy nature of our sample. These fragile glasses have also been found for some polymeric systems [71]. The deviation of VFT fit from the experimental data in the higher temperature range is further analyzed as discussed below. It has also been reported that a poorer fit to the experimental data is expected for more fragile liquid [54].

The linearized derivative-based analysis, first proposed by Stickel *et al.* [72], was performed to emphasize subtle changes in the dependence of relaxation time τ on temperature. It has been shown that the plot of $T\ [d(\ln\tau)/d(1/T)]^{-1/2}$ vs T should give rise to a linear dependence in the region where the VFT equation is valid [69]. For our sample, linear temperature dependence with two different slopes was found in the low- and high-temperature regions, as shown in Fig. 9. The crossover temperature T_B was found to be at about 370 K, which separates the two dynamical regimes. This analysis shows that the VFT relation is more appropriate to describe the temperature variation of the relaxation frequency for our sample.

It has been shown in many cases of liquid crystalline glassformers [70,73,74] that $\tau = \tau_0(T - T_x)^{-\gamma}$ can be used to portray the behavior of relaxation in accordance with the mode coupling theory (MCT) [75,76]. Here T_x denotes the MCT singular temperature describing a hypothetical crossover from the ergodic to the nonergodic regime, and the exponent $2 < \gamma < 4$ is a nonuniversal parameter [75]. However, for our sample, we found that the temperature variation of the relaxation frequency can be fitted best with the VFT relation given by Eq. (5).

The DSC measurements were carried out to measure the possible glass transition in the cooling and heating cycle of the sample at different rates. The observed DSC thermograms are shown in Fig. 10. A step change in the DSC thermogram corresponding to the glass transition was detected on both the cooling and heating cycles. The vitrification temperature (T_g) on cooling at a rate of 20 K/min was 271 K, and the corresponding glass softening temperature on heating was 268 K. These temperatures were determined from the inflection point of the DSC thermogram corresponding to the half height of the step in the heat flow curve. The difference between calorimetric glass transition temperature T_g and Vogel temperature T_0 is about 18 K for our sample, which is considered to be low as expected for highly fragile systems [54]. This difference tends to zero for magnetic relaxation in spin glasses [77].

Now we discuss the possible origin of the observed M_1 mode in our sample. The dielectric relaxation processes can be divided broadly into two categories: noncollective and collective dynamics of the molecules. When the rotational dynamics of the individual molecules are not correlated, the liquid crystal molecules themselves can exhibit two dielectric relaxation mechanisms linked to the rotation of the molecules about their long and short axes. The former generally occurs in the GHz frequency range, while the latter occurs at relatively lower frequencies. Particularly when dealing with BC molecules, the relaxation mode associated with molecular rotation about the short axis lies in the range of tens of kHz [78,79]. Moreover, a number of distinguishable dispersions have been observed for BC compounds, the origins of which are not yet clear [78]. For the glass-forming system, the relaxation frequencies

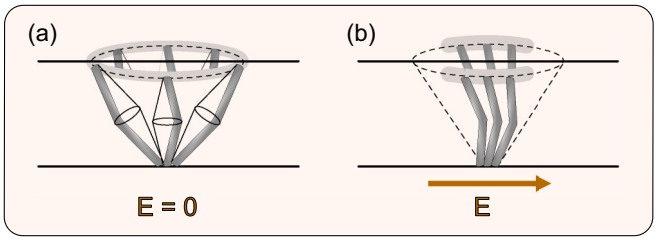

FIG. 11. Schematic representation for the arrangement of bent-core molecules in a layer of the dSmA phase (a) without electric field and (b) in the presence of the field applied parallel to the smectic layer. The change in the molecular distribution on the application of field gives rise to collective mode M_1 observed in our sample.

associated with these dispersions are expected to decrease rapidly near the glass transition. However, in the case of our compound, only one relaxation mode M_1 was observed. This observation suggests that the M_1 mode can possibly arise either due to the noncollective rotation of the molecules about their short axes or due to some collective molecular movement.

Although the BTCN8 molecules have nonzero dipole moments, our experimental studies confirmed the absence of spontaneous polarization in the observed smectic phases. Furthermore, we didn't find experimental evidence of Langevin-type ordering of the dipole moments in the smectic layers [14]. Therefore, mode M_1 is not associated with the collective polar ordering of the molecules in our sample.

Based on the molecular configuration in the dSmA and the SmC phases, we propose a possible collective mechanism that gives rise to the M_1 mode. In the dSmA phase, the long axes of the molecules are distributed uniformly on a cone about the layer normal [see Fig. 11(a)]. Under the application of a small electric field in the plane of the smectic layers, the molecules reorient azimuthally on the cone, resulting in a weak biaxiality in the system. Due to the strong transverse component of the dipole moment of the molecules, the sample has negative dielectric anisotropy, and the field tends to redistribute the molecules on the cone along the directions perpendicular to the applied field as shown in Fig. 11(b). The observed relaxation mode M_1 in our sample can be attributed to this collective redistribution of the molecules on the cone. In the SmC phase, the molecular distribution around the cone is peaked at a preferred azimuthal angle, giving rise to a nonzero optical tilt. The optical tilt increases with decreasing temperature in the SmC phase. However, the molecules still have a broad distribution along the azimuthal direction. This is also supported by the fact that the optical tilt angle in the SmC phase is about 15° at ambient temperature, which is significantly smaller than the corresponding intralayer molecular tilt measured from XRD studies (∼33°). Hence, a similar molecular redistribution confining them in the plane perpendicular to the applied field is expected to occur in the planar-aligned SmC phase. Thus, the relaxation frequency of the mode M_1 varies continuously across the transition from the dSmA to the SmC phase and persists throughout the SmC phase. The relaxation frequency of mode M_1 decreases gradually with decreasing temperature, indicating that this molecular redistribution about the cone tends to be frozen. The relaxation frequency starts to decline rapidly in the lower temperature region of the SmC phase because of the experimentally confirmed glassy behavior of our sample.

The broad molecular distribution on the tilt cone also explains the increase in birefringence of the SmC phase under the application of a relatively higher field of about 2 V/μm, as observed in POM studies (see Fig. S3 [62]). The applied field confines the molecules in the plane of the LC cell. This results in the increased order parameters and, hence, the birefringence of the sample. This field induced change is reversible as the molecules relax back to their original distribution after removal of the field. Further detailed experimental studies are required to confirm the exact mechanism giving rise to the observed mode M_1.

The constituent molecules of the compound BTCN8 have a central thiophene ring, which gives rise to an opening angle of about 143°, which is larger than 120° typically found for bent-core molecules. This perhaps can be attributed to the absence of net polarization in the observed smectic phases. We do not see any sign of the B2 phase typically exhibited by bent-core molecules. Rather, the observed phases are calamatic phases generally observed for rodlike molecules.

IV. CONCLUSION

We report experimental studies on a compound consisting of bent-core banana-shaped molecules, which exhibits the following enantiotropic liquid crystalline phases on cooling: Isotropic → Nematic → dSmA → SmC → Smectic Glass. The XRD studies show the minimal layer contraction across the dSmA to the SmC transition, and the POM studies further confirmed the "de Vries" nature of the SmA phase. The switching current measurements indicate the absence of spontaneous polarization in both the smectic phases. A dielectric relaxation mode was observed due to the reorientation of the molecules on the tilt cone in the dSmA phase, and it persists in the lower temperature SmC phase. The relaxation frequency of this mode decreases rapidly with decreasing temperature following the VFT equation, indicating a fragile glassy behavior of our sample. The DSC measurements confirmed the glass transition at about 271 K, which does not depend significantly on the cooling rate. We have proposed a model for the observed dielectric mode in the dSmA phase to account for experimental results. Interestingly, the studied bent-core compound has the unique property of exhibiting a de Vries SmA phase along with the glassy behavior.

ACKNOWLEDGMENTS

We thank Ms. Vasudha K. N. for her help in acquiring DSC and XRD data. We also thank Dr. T. Narasimhaswamy for his support with the chemical synthesis of the compound.

[1] S. Chandrasekhar, *Liquid Crystals*, 2nd ed. (Cambridge University Press, Cambridge, 1992).

[2] T. P. Rieker, N. A. Clark, G. S. Smith, D. S. Parmar, E. B. Sirota, and C. R. Safinya, "Chevron" local layer structure in

surface-stabilized ferroelectric smectic-*c* cells, Phys. Rev. Lett. **59**, 2658 (1987).

[3] L. Limat and J. Prost, A model for the chevron structure obtained by cooling a smectic A liquid crystal in a cell of finite thickness, Liq. Cryst. **13**, 101 (1993).

[4] N. A. Clark and S. T. Lagerwall, Submicrosecond bistable electro-optic switching in liquid crystals, Appl. Phys. Lett. **36**, 899 (1980).

[5] J. P. F. Lagerwall and F. Giesselmann, Current topics in smectic liquid crystal research, ChemPhysChem **7**, 20 (2006).

[6] A. De Vries, A. Ekachai, and N. Spielberg, Why the molecules are tilted in all smectic A phases, and how the layer thickness can be used to measure orientational disorder, Mol. Cryst. Liq. Cryst. **49**, 143 (1979).

[7] A. de Vries, The description of the smectic A and C phases and the smectic A-C phase transition of TCOOB with a diffuse-cone model, J. Chem. Phys. **71**, 25 (1979).

[8] S. K. Prasad, D. S. Shankar Rao, S. Sridevi, C. V. Lobo, B. R. Ratna, J. Naciri, and R. Shashidhar, Unusual dielectric and electrical switching behavior in the de Vries smectic *A* phase of two organosiloxane derivatives, Phys. Rev. Lett. **102**, 147802 (2009).

[9] J. C. Roberts, N. Kapernaum, Q. Song, D. Nonnenmacher, K. Ayub, F. Giesselmann, and R. P. Lemieux, Design of liquid crystals with "de Vries-like" properties: Frustration between SmA- and SmC-promoting elements, J. Am. Chem. Soc. **132**, 364 (2010).

[10] H. G. Yoon, D. M. Agra-Kooijman, K. Ayub, R. P. Lemieux, and S. Kumar, Direct observation of diffuse cone behavior in de Vries smectic-*A* and -*C* phases of organosiloxane mesogens, Phys. Rev. Lett. **106**, 087801 (2011).

[11] C. P. J. Schubert, C. Müller, A. Bogner, F. Giesselmann, and R. P. Lemieux, Design of liquid crystals with 'de Vries-like' properties: structural variants of carbosilane-terminated 5-phenylpyrimidine mesogens, Soft Matter **13**, 3307 (2017).

[12] H. Ocak, B. Bilgin-Eran, M. Prehm, S. Schymura, J. P. F. Lagerwall, and C. Tschierske, Effects of chain branching and chirality on liquid crystalline phases of bent-core molecules: Blue phases, de Vries transitions and switching of diastereomeric states, Soft Matter **7**, 8266 (2011).

[13] S. P. Sreenilayam, Y. P. Panarin, J. K. Vij, V. P. Panov, A. Lehmann, M. Poppe, M. Prehm, and C. Tschierske, Spontaneous helix formation in non-chiral bent-core liquid crystals with fast linear electro-optic effect, Nat. Commun. **7**, 11369 (2016).

[14] A. A. S. Green, M. R. Tuchband, R. Shao, Y. Shen, R. Visvanathan, A. E. Duncan, A. Lehmann, C. Tschierske, E. D. Carlson, E. Guzman *et al.*, Chiral incommensurate helical phase in a smectic of achiral bent-core mesogens, Phys. Rev. Lett. **122**, 107801 (2019).

[15] Y. P. Panarin, S. P. Sreenilayam, V. Swaminathan, C. Tschierske, and J. K. Vij, Observation of an anomalous SmA-SmC-SmA phase sequence in a bent-core liquid crystal derived from 4-cyanoresorcinol, Phys. Rev. Res. **2**, 013118 (2020).

[16] S. Kaur, A. Barthakur, G. Mohiuddin, S. P. Gupta, S. Dhara, and S. K. Pal, Observation of "de Vries-like" properties in bent-core molecules, Chem. Sci. **13**, 2249 (2022).

[17] T. Niori, T. Sekine, J. Watanabe, T. Furukawa, and H. Takezoe, Distinct ferroelectric smectic liquid crystals consisting of banana shaped achiral molecules, J. Mater. Chem. **6**, 1231 (1996).

[18] D. R. Link, G. Natale, R. Shao, J. E. Maclennan, N. A. Clark, E. Körblova, and D. M. Walba, Spontaneous formation of macroscopic chiral domains in a fluid smectic phase of achiral molecules, Science **278**, 1924 (1997).

[19] A. Jákli, O. D. Lavrentovich, and J. V. Selinger, Physics of liquid crystals of bent-shaped molecules, Rev. Mod. Phys. **90**, 045004 (2018).

[20] H. Takezoe and A. Eremin, *Bent-Shaped Liquid Crystals: Structures and Physical Properties* (CRC Press, Boca Raton, FL, 2019).

[21] T. Sekine, Y. Takanishi, T. Niori, and J. W. Takezoe, Ferroelectric properties in banana-shaped achiral liquid crystalline molecular systems, Jpn. J. Appl. Phys. **36**, L1201 (1997).

[22] A. Eremin, S. Diele, G. Pelzl, H. Nádasi, W. Weissflog, J. Salfetnikova, and H. Kresse, Experimental evidence for an achiral orthogonal biaxial smectic phase without in-plane order exhibiting antiferroelectric switching behavior, Phys. Rev. E **64**, 051707 (2001).

[23] R. A. Reddy, C. Zhu, R. Shao, E. Korblova, T. Gong, Y. Shen, E. Garcia, M. A. Glaser, J. E. Maclennan, D. M. Walba, and N. A. Clark, Spontaneous ferroelectric order in a bent-core smectic liquid crystal of fluid orthorhombic layers, Science **332**, 72 (2011).

[24] D. Coleman, J. Fernsler, N. Chattham, M. Nakata, Y. Takanishi, E. Körblova, D. R. Link, R.-F. Shao, W. Jang, J. Maclennan *et al.*, Polarization-modulated smectic liquid crystal phases, Science **301**, 1204 (2003).

[25] N. Vaupotič, M. Čopič, E. Gorecka, and D. Pociecha, Modulated structures in bent-core liquid crystals: Two faces of one phase, Phys. Rev. Lett. **98**, 247802 (2007).

[26] D. K. Yoon, R. Deb, D. Chen, E. Körblova, R. Shao, K. Ishikawa, N. V. S. Rao, D. M. Walba, I. I. Smalyukh, and N. A. Clark, Organization of the polarization splay modulated smectic liquid crystal phase by topographic confinement, Proc. Natl. Acad. Sci. USA **107**, 21311 (2010).

[27] N. Chattham, M.-G. Tamba, R. Stannarius, E. Westphal, H. Gallardo, M. Prehm, C. Tschierske, H. Takezoe, and A. Eremin, Leaning-type polar smectic-*c* phase in a freely suspended bent-core liquid crystal film, Phys. Rev. E **91**, 030502(R) (2015).

[28] V. D. Mishra, H. T. Srinivasa, and A. Roy, Leaning induced layer undulated tilted smectic phase of asymmetric bent-core liquid crystals, J. Chem. Phys. **158**, 074906 (2023).

[29] L. E. Hough, M. Spannuth, M. Nakata, D. A. Coleman, C. D. Jones, G. Dantlgraber, C. Tschierske, J. Watanabe, E. Körblova, D. M. Walba *et al.*, Chiral isotropic liquids from achiral molecules, Science **325**, 452 (2009).

[30] Y. Takanishi, T. Izumi, J. Watanabe, K. Ishikawa, H. Takezoe, and A. Iida, Field-induced molecular reorientation keeping a frustrated structure in an achiral bent-shaped liquid crystal, J. Mater. Chem. **9**, 2771 (1999).

[31] K. Pelz, W. Weissflog, U. Baumeister, and S. Diele, Various columnar phases formed by bent-core mesogens, Liq. Cryst. **30**, 1151 (2003).

[32] C. L. Folcia, J. Etxebarria, J. Ortega, and M. B. Ros, Structural study of a bent-core liquid crystal showing the B_1-B_2 transition, Phys. Rev. E **74**, 031702 (2006).

[33] H. R. Zeller, Dielectric relaxation and the glass transition in nematic liquid crystals, Phys. Rev. Lett. **48**, 334 (1982).

[34] S. J. Rzoska, M. Paluch, S. Pawlus, A. Drozd-Rzoska, J. Ziolo, J. Jadzyn, K. Czuprynski, and R. Dabrowski, Complex

dielectric relaxation in supercooling and superpressing liquid-crystalline chiral isopentylcyanobiphenyl, Phys. Rev. E **68**, 031705 (2003).
[35] I. Dierking, Experimental investigations of a chiral smectic glass-forming liquid crystal, Liq. Cryst. **35**, 1015 (2008).
[36] J. Wu, T. Usui, and J.-i. Hanna, Synthesis of a novel smectic liquid crystalline glass and characterization of its charge carrier transport properties, J. Mater. Chem. **21**, 8045 (2011).
[37] M. Tarnacka, K. Adrjanowicz, E. Kaminska, K. Kaminski, K. Grzybowska, K. Kolodziejczyk, P. Wlodarczyk, L. Hawelek, G. Garbacz, A. Kocot, and M. Paluch, Molecular dynamics of itraconazole at ambient and high pressure, Phys. Chem. Chem. Phys. **15**, 20742 (2013).
[38] M. Jasiurkowska-Delaporte, S. Napolitano, J. Leys, E. Juszyńska-Gałazka, M. Wübbenhorst, and M. Massalska-Arodź, Glass transition dynamics and crystallization kinetics in the smectic liquid crystal 4-*n*-butyloxybenzylidene-4′-*n*′-octylaniline (BBOA), J. Phys. Chem. B **120**, 12160 (2016).
[39] A. Deptuch, S. Lalik, M. Jasiurkowska-Delaporte, E. Juszyńska-Gałazka, A. Drzewicz, M. Urbańska, and M. Marzec, Comparative study of electrooptic, dielectric, and structural properties of two glassforming antiferroelectric mixtures with a high tilt angle, Phys. Rev. E **105**, 024705 (2022).
[40] S. Rauch, C. Selbmann, P. Bault, H. Sawade, G. Heppke, O. Morales-Saavedra, M. Y. M. Huang, and A. Jákli, Glass forming banana-shaped compounds: Vitrified liquid crystal states, Phys. Rev. E **69**, 021707 (2004).
[41] C. J. Klok, Biological glass: A strategy to survive desiccation and heat, J. Exp. Biol. **213**, iv (2010).
[42] F. B. Wadsworth, M. J. Heap, D. E. Damby, K.-U. Hess, J. Najorka, J. Vasseur, D. Fahrner, and D. B. Dingwell, Local geology controlled the feasibility of vitrifying Iron Age buildings, Sci. Rep. **7**, 40028 (2017).
[43] J. Pagacz, P. Stach, L. Natkaniec-Nowak, B. Naglik, and P. Drzewicz, Preliminary thermal characterization of natural resins from different botanical sources and geological environments, J. Therm. Anal. Calorim. **138**, 4279 (2019).
[44] M. Petters and S. Kasparoglu, Predicting the influence of particle size on the glass transition temperature and viscosity of secondary organic material, Sci. Rep. **10**, 15170 (2020).
[45] N. R. Jadhav, V. L. Gaikwad, K. J. Nair, and H. M. Kadam, Glass transition temperature: Basics and application in pharmaceutical sector, Asian J. Pharmaceutics (AJP) **3**, 82 (2009).
[46] Y. H. Roos, Glass transition temperature and its relevance in food processing, Annu. Rev. Food Sci. Technol. **1**, 469 (2010).
[47] H. T. H. Nguyen, P. Qi, M. Rostagno, A. Feteha, and S. A. Miller, The quest for high glass transition temperature bioplastics, J. Mater. Chem. A **6**, 9298 (2018).
[48] J. H. Crowe, J. F. Carpenter, and L. M. Crowe, The role of vitrification in anhydrobiosis, Annu. Rev. Physiol. **60**, 73 (1998).
[49] J. M. V. Blanshard and P. Lillford, *The Glassy State in Foods* (Nottingham University, Press, Loughborough, England, 1993).
[50] A. L. Greer, Metallic Glasses, Science **267**, 1947 (1995).
[51] P. G. Debenedetti and F. H. Stillinger, Supercooled liquids and the glass transition, Nature (London) **410**, 259 (2001).
[52] F. Kremer and A. Schönhals (eds.), *Broadband Dielectric Spectroscopy* (Springer, Berlin, Heidelberg, 2003).
[53] K. Ngai, *Relaxation and Diffusion in Complex Systems*, Partially Ordered Systems (Springer, New York, 2011).
[54] C. A. Angell, Formation of glasses from liquids and biopolymers, Science **267**, 1924 (1995).
[55] J. C. Dyre, Colloquium: The glass transition and elastic models of glass-forming liquids, Rev. Mod. Phys. **78**, 953 (2006).
[56] R. Elschner, R. Macdonald, H. J. Eichler, S. Hess, and A. M. Sonnet, Molecular reorientation of a nematic glass by laser-induced heat flow, Phys. Rev. E **60**, 1792 (1999).
[57] R. Teerakapibal, C. Huang, A. Gujral, M. D. Ediger, and L. Yu, Organic glasses with tunable liquid-crystalline order, Phys. Rev. Lett. **120**, 055502 (2018).
[58] Z. Chen, J. Yu, R. Teerakapibal, L. Meerpoel, R. Richert, and L. Yu, Organic glasses with tunable liquid-crystalline order through kinetic arrest of end-over-end rotation: The case of saperconazole, Soft Matter **16**, 2025 (2020).
[59] K. Miyasato, S. Abe, H. Takezoe, A. Fukuda, and E. Kuze, Direct method with triangular waves for measuring spontaneous polarization in ferroelectric liquid crystals, Jpn. J. Appl. Phys. **22**, L661 (1983).
[60] G. Pratap, D. Malkar, E. Varathan, N. P. Lobo, A. Roy, and T. Narasimhaswamy, 3-cyano thiophene-based π-conjugated mesogens: XRD and ^{13}C NMR investigations, Liq. Cryst. **46**, 680 (2019).
[61] A. S. Govind and N. V. Madhusudana, A simple molecular theory of smectic-C liquid crystals, Europhys. Lett. **55**, 505 (2001).
[62] See Supplemental Material at http://link.aps.org/supplemental/10.1103/PhysRevE.109.024703 for the measurement of optical tilt angle, the results of switching current measurements; details of electro-optic studies, and the frequency dependence of dielectric constant measured for sample between homeotropic LC cell. The Supplemental Material also contains Ref. [59].
[63] Q. Song, D. Nonnenmacher, F. Giesselmann, and R. P. Lemieux, Tuning 'de Vries-like' properties in siloxane- and carbosilane-terminated smectic liquid crystals, J. Mater. Chem. C **1**, 343 (2013).
[64] H. Kumar Singh, S. Kumar Singh, R. Nandi, D. S. Shankar Rao, S. Krishna Prasad, R. K. Singh, and B. Singh, Observation of exceptional 'de Vries-like' properties in a conventional aroylhydrazone based liquid crystal, RSC Adv. **6**, 57799 (2016).
[65] S. Havriliak and S. Negami, A complex plane analysis of α-dispersions in some polymer systems, J. Polym. Sci. C: Polym. Symp. **14**, 99 (1966).
[66] S. Havriliak and S. Negami, A complex plane representation of dielectric and mechanical relaxation processes in some polymers, Polymer **8**, 161 (1967).
[67] D. W. Davidson and R. H. Cole, Dielectric relaxation in glycerol, propylene glycol, and *n*-propanol, J. Chem. Phys. **19**, 1484 (1951).
[68] K. S. Cole and R. H. Cole, Dispersion and absorption in dielectrics I. Alternating current characteristics, J. Chem. Phys. **9**, 341 (1941).
[69] A. Drozd-Rzoska and S. J. Rzoska, Derivative-based analysis for temperature and pressure evolution of dielectric relaxation times in vitrifying liquids, Phys. Rev. E **73**, 041502 (2006).
[70] A. Drozd-Rzoska, S. J. Rzoska, and S. Starzonek, New scaling paradigm for dynamics in glass-forming systems, Prog. Mater. Sci. **134**, 101074 (2023).

[71] C. A. Angell, L. Monnerie, and L. M. Torell, Strong and fragile pehavior in liquid polymers, MRS Online Proc. Library **215**, 3 (1990).

[72] F. Stickel, E. W. Fischer, and R. Richert, Dynamics of glass-forming liquids. II. Detailed comparison of dielectric relaxation, dc-conductivity, and viscosity data, J. Chem. Phys. **104**, 2043 (1996).

[73] S. Rzoska, M. Paluch, A. Drozd-Rzoska, J. Ziolo, P. Janik, and K. Czupryński, Glassy and fluidlike behavior of the isotropic phase of *n*-cyanobiphenyls in broad-band dielectric relaxation studies, Eur. Phys. J. E **7**, 387 (2002).

[74] A. Drozd-Rzoska, Universal behavior of the apparent fragility in ultraslow glass forming systems, Sci. Rep. **9**, 6816 (2019).

[75] W. Gotze and L. Sjogren, Relaxation processes in supercooled liquids, Rep. Prog. Phys. **55**, 241 (1992).

[76] A. Schönhals, F. Kremer, A. Hofmann, E. W. Fischer, and E. Schlosser, Anomalies in the scaling of the dielectric α-relaxation, Phys. Rev. Lett. **70**, 3459 (1993).

[77] J. Souletie, The glass transition: Dynamic and static scaling approach, J. Phys. France **51**, 883 (1990).

[78] P. Salamon, N. Éber, Á. Buka, J. T. Gleeson, S. Sprunt, A. JákliDielectric properties of mixtures of a bent-core and a calamitic liquid crystal, Phys. Rev. E **81**, 031711 (2010).

[79] L. Marino, A. T. Ionescu, S. Marino, N. ScaramuzzaDielectric investigations on a bent-core liquid crystal, J. Appl. Phys. **112**, 114113 (2012).